The Electromagnetic Calorimeter of the HERA – B experiment

G. Avoni [a], C. Baldanza [a], A. Bertin [a], B. Bobchenko [b], M. Bruschi [a], I. D'Antone [a], S. De Castro [a], L. Fabbri [a], P. Faccioli [a], J. Flammer [c], B. Giacobbe [a], Yu. Gilitsky [d], P. Giovannini [a], A. Golutvin [b], O. Gouchtchine [b], I. Lax [a], I. Massa [a], I. Machikhiliyan [b], S. Meneghini [a], Yu. Mikhailov [d], E. Novikov [b], M. Piccinini [a], M. Rizzi [a], V. Rusinov [b], C. Sbarra [a], A. Sbrizzi [a], N. Semprini-Cesari [a], S. Shuvalov [e], A. Soldatov [d], R. Spighi [a], E. Tarkovsky [b], M. Villa [a], A. Vitale [a], A. Zoccoli [a], and M. Zuffa [a]

[a] *Dipartimento di Fisica della Università di Bologna and INFN Sezione di Bologna, I-40126 Bologna, Italy*

[b] *Institute of Theoretical and Experimental Physics, B. Cheremushkinskaya 25, Moscow 117259, Russia*

[c] *CERN, Geneva, Switzerland*

[d] *Institute of High Energy Physics, RU-142248, Protvino, (Moscow), Russia*

[e] *Institut für Physik, Humboldt Universität zu Berlin, Newtonstr.15, D-12489 Berlin, Germany* [1]

PACS: 29.40.Vj, 78.70.-g, 25.40.-h, 06.20.Fn
Keywords: proton-Nucleus interactions; calorimetry; Bremsstrahlung.

Abstract

The electromagnetic calorimeter of the HERA – B experiment built at the HERA proton accelarator at DESY (Hamburg) is described. The construction characteristics of the detector, of the related front-end, readout, trigger and service electronics are discussed together with the constraints and the motivations which inspired the design philosophy. The detector performance are presented as obtained from the analysis of the data acquired during the HERA – B running period, including calibration procedures and achievements and the electron identification capability exploiting a method, proposed here for the first time, based on the observation of the associated bremsstrahlung γ. Finally some observed physical signals and a short overview of the main obtained physics results are presented.

Preprint submitted to Elsevier Science

1 The HERA – B experiment

The HERA – B experiment [1] was a fixed target experiment studying the interactions of the 920 GeV protons, provided by the HERA accelerator, on target wires of different materials. A sketch of the detector can be found in Fig. 1.

The physics program included the field of heavy-quark physics and QCD studies, in particular charmonium (J/ψ, χ_c and ψ') production, open-charm cross section measurement, multi-quark state search, b-quark physics, hard photon production, etc.

A major part of the program required the selection of the lepton decays of the J/ψ particle in a physics environment characterized by a large background, typical of the hadronic interactions, and small production cross sections of the interesting reactions, being the typical signal over background ratio of the order of 10^{-6}. This required a highly efficient J/ψ selection with a large background rejection, obtained thanks to very selective di-electron and di-muon triggers and suitable lepton identification and reconstruction capabilities. These requirements together with the constraint imposed by the radiation levels were the main guidelines to the design of the detector and, inside it, of the electromagnetic calorimeter (ECAL).

[1] supported by the Bundesministerium für Bildung und Forschung

1.1 The ECAL physics goals

ECAL [1][2][3] was designed to perform the following main tasks:

- to provide 0-level (pre-trigger, PT) electron candidates to the first-level trigger (FLT) of the experiment. The needed background suppression ($\sim 10^5$) was obtained thanks to a multi-level, pipelined, almost dead-timeless trigger scheme, to which the ECAL and the MUON detectors provided the initial seeds [1];
- to detect and reconstruct electrons and photons providing a suitable particle identification (PID) and hadron rejection. Electron/positron ($e^{\pm}$) and photon (γ) PID were provided by exploiting both classical algorithms, such as E/p ($e^{\pm}$) and cluster shape ($e^{\pm}, \gamma$), and a completely new and original electron tagging method based on the detection of the γ emitted for bremsstrahlung, also applied at trigger level. Such algorithms needed suitable spatial and energy reconstruction capabilities.
- to monitor on-line the interaction rate by means of the features implemented in the firmware of the pretrigger electronics. The ECAL information is also used, in combination with other detectors, for measuring the integrated acquired luminosity with an original method described in [4].

In Sect. 2 the ECAL general design and structure are outlined and the radiation environment in which it operated is discussed. The front-end,

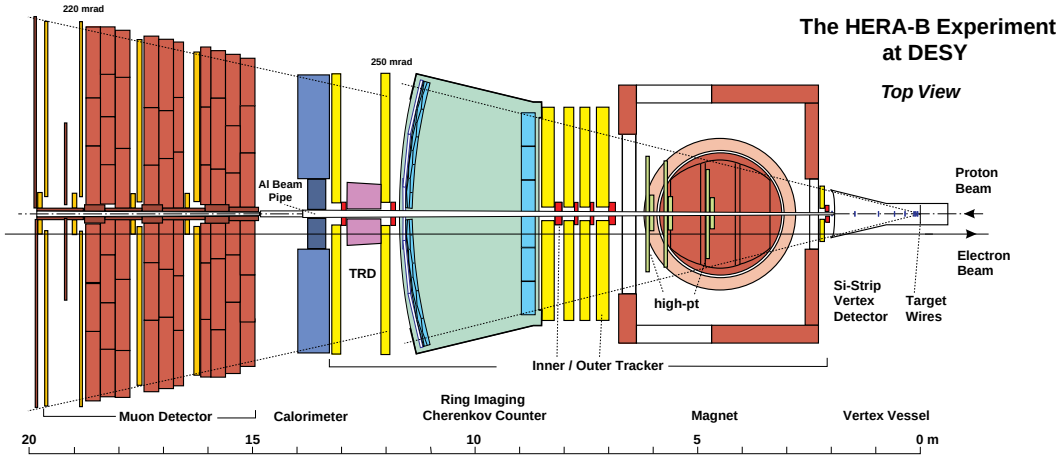

Fig. 1. Scheme of the HERA – B detector

readout and pretrigger electronics are described in Sect. 3, 4 and 5, while in Sect. 6 and 7 the software for reconstruction and the calibration procedure are discussed. In Sect. 8 and 10 the ECAL performance and the main physical results obtained are shown.

2 The ECAL design

ECAL was positioned $\sim$ 13.5 m downstream the HERA – B wire target and was designed in order to operate in the following conditions:

- maximum charged track occupancy per cell $\sim$ 10% (at 4 interactions per bunch crossing i.e. 40 MHz interaction rate (i.r.));
- transverse energy deposition per cell in the 0-6 GeV range (except 16 modules around beam pipe (see Fig. 2) whose dynamic range was adjusted to 250 GeV).

In order to cope with the first condition, the calorimeter was structured in 3 sections (INNER, MIDDLE and OUTER, see Fig. 2) with a different granularity in order to follow the steep radial dependence of track density in the HERA – B environment. All sections employed the same "shashlik" technology [5] of a sampling scintillator/absorber sandwich structure. This technology provides an economic solution for large size calorimeters ensuring, at the same time, good performance and uniformity of response. Moreover adequate signal time characteristics and easy precise calibration can be achieved.

The basic elements were 2344 modules of transverse dimensions 11.2 $\times$ 11.2 cm^2. The different granularity was obtained by subdividing the modules of the INNER section in a matrix of 5 $\times$ 5 cells and the ones of the MIDDLE section in 2 $\times$ 2 matrices, while in the OUTER section modules were not segmented, adding up to 5956 individually read out channels. Within the INNER section, an INNERMOST part was defined (see Fig. 2), differing from the rest of the section in terms of front-end and monitoring electronics, due to

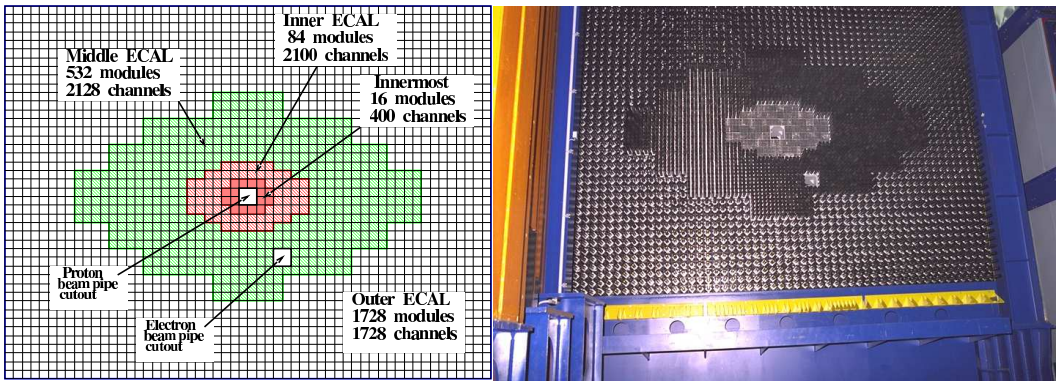

Fig. 2. The HERA – B Electromagnetic Calorimeter structure

the high radiation environment close to the beam pipe.

2.1 Radiation environment

The HERA – B detector had to cope with a large radiation environment, typical of the hadronic interactions at high energy, strongly depending on the distance from the beam pipe.

The INNERMOST part of the calorimeter was designed to cope with up to $\sim 50\ kGy$ (at shower-max position) dose per year of operation while the same numbers for the INNER, MIDDLE and OUTER sections are respectively ~ 20, ~ 4 and $\sim 1\ kGy/year$. For this reason a different technology was used in particular for the signal collection devices.

2.2 The INNER section

The schematic construction of the INNER ECAL module is shown in Fig. 3.

The stack of absorber/scintillator tiles consisted of 40 layers, each made of an absorber plate 2.2 mm thick and a scintillator plate 1 mm thick, corresponding, in total, to 23 X_0. The small lateral cell size ($\sim 2.5 \times 2.5\ cm^2$) and the need of containing the lateral development of electromagnetic showers in order to separate signals in the high particle density region close to the beam pipe imposed the choice of a W-Ni-Fe alloy as absorber, thanks to its small Molière radius (see Tab. 1).

Due to severe radiation environment, modules exploited radiation hard scintillator based on PSM115, separated from the absorber plate by a 0.1 mm TYVEK paper sheet to improve the light collection, to provide uniform mechanical load onto scintillator tiles and to ensure elasticity to the assembled stack. Tile edges were aluminized to prevent tile-to-tile light cross-talk and to improve light collection. The rigidity of the complete stack was ensured by 0.12 mm stainless steel bands pretensioned and welded to front and rear steel lids.

The light produced by scintillators was collected by nine 1.2 mm di-

ameter KURARAY-Y11 radiation hard wavelength-shifter (WLS) fibres penetrating the entire length of the cell, and transported to the readout photomultipliers window. Holes of 1.5 mm diameter for the WLS fibres were arranged on a square uniform lattice. Fibres for each cell were bound together, polished and coupled to their PM through 1 mm air gap. At the front of the cell, fibres were cut and aluminized. Radiation tests of module parts showed that light-yield loss under irradiation did not exceed 20% at acquired dose of 50 kGy [6].

The 25 PMs, together with power supplies, were mounted inside a rigid aluminum housing at the rear of the module. The front surface of the module was closed by the printed circuit board (PCB) of the monitoring system equipped with 25 Light Emission Diodes (LED) faced to the central fibre of each cell. The light from LED was injected into WLS fibre through the small hole drilled in the center of aluminized fibre edge.

The average amount of light produced in the INNER ECAL cells was equivalent to $\sim$ 130 photoelectrons (p.e) per 1 GeV of deposited energy.

2.3 The MIDDLE and OUTER sections

A MIDDLE ECAL module is shown schematically in Fig. 4. The main differences with respect to the INNER were:

- the absorber/scintillator stack consisted of 37 layers each made of a lead absorber plate 3 mm thick and scintillator tiles 6 mm thick, corresponding, in total, to 20 X_0;
- each of the four cells in the module housed 18 U-shaped WLS fibres inserted into the holes of the scintillator/absorber stack;
- PMs and power supplies were housed inside the steel cylindrical tubes attached to the back side of the module;
- light signal from LED test system was injected into an additional straight fibre positioned at the center of each cell (not shown in the picture).

OUTER modules shared the same design, but scintillator tiles had full module transverse size and only one tube for PM housing was present in the module axis.
Both for MIDDLE and OUTER modules, less radiation tolerant Bicron BCF-91A WLS fibres were used due to the lower expected deposited dose with respect to the INNER case [6].

The average amount of light produced in the MIDDLE (OUTER) ECAL cells was equivalent $\sim$ 800 p.e. ($\sim$ 1300 p.e.) per 1 GeV of deposited energy.

All relevant modules parameters are reported in Table 1.

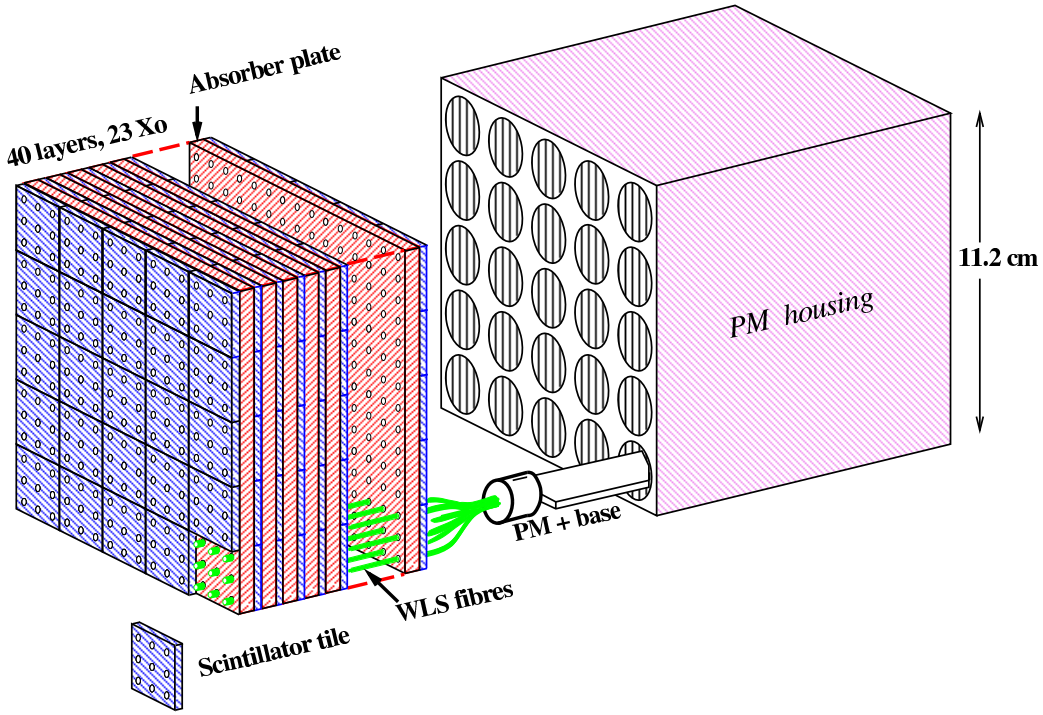

Fig. 3. INNER ECAL module structure.

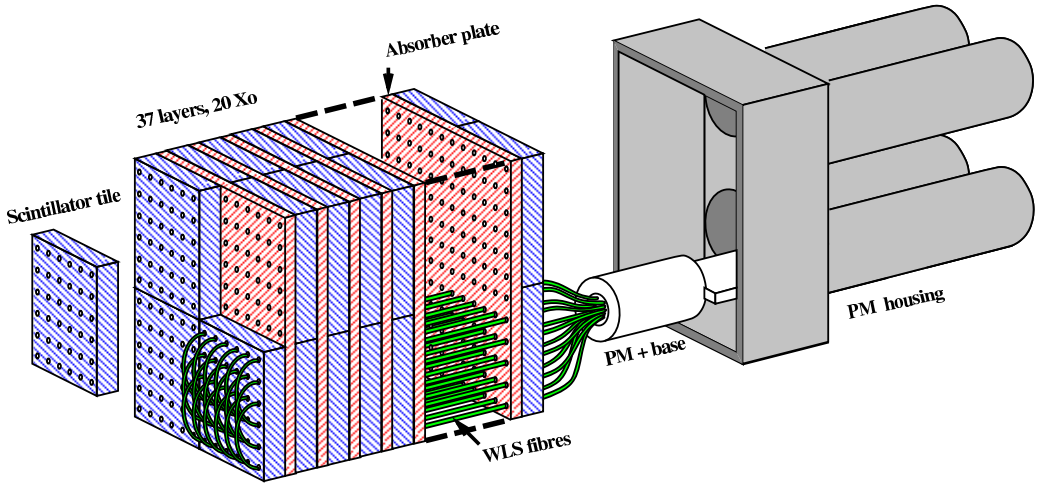

Fig. 4. MIDDLE ECAL module structure

3 The front-end and monitoring electronics

3.1 Photodetectors and power supplies

The large amount of light (see Table 1) produced in ECAL modules allowed to use ordinary photomultipliers (phototubes, PMs) to readout the light collected by WLS fibres. PMs and their power supplies had to satisfy the following specifications:

(1) to have a photocathode sensitive to the green light of WLS fibres (490 nm) with quantum

	INNERMOST/INNER	MIDDLE	OUTER
Channels	2100	2128	1728
Cell size	2.23 cm	5.59 cm	11.18 cm
Absorber	W-Ni-Fe alloy	lead (Pb)	lead (Pb)
Radiation Length (X_0)	0.558 cm	1.675 cm	1.675 cm
Equiv. Molière rad.	1.24 cm	4.15 cm	4.15 cm
Depth	13 cm (23 X_0)	34 cm (20 X_0)	34 cm (20 X_0)
Volume ratio	W:Sc = 2.2:1	Pb:Sc = 1:2	Pb:Sc = 1:2
WLS	Kuraray Y-11	BCF-91A	BCF-91A
Light yield (p.e./ GeV)	130	800	1300
PM type	R-5600/FEU68	FEU-84-3	FEU-84-3
LED (wavelength, nm)	Marl (450)	L934SRCB (660)	L934SRCB (660)
Max. radiation dose (kGy/year) at shower-max	50/20	4	1

Table 1
HERA – B ECAL parameters.

efficiency large enough to avoid deterioration of ECAL energy resolution due to photo statistics effects;

(2) to have proper transverse dimensions matching the cell size and the cross-section of the WLS fibres bundle in the front of the tower;

(3) to have sufficient radiation resistance, especially in case of INNERMOST region (maximum radiation dose at PM plane was 15 $kG/year$);

(4) to operate reliably in the stray magnetic fields (about few tens Gauss);

(5) to provide good linearity of response ($\sim 2\%$) up to 10 mA output currents.

Three different PM types were chosen to instrument the INNERMOST (HAMAMATSU R-5600), INNER (Russian FEU-68) and MIDDLE/OUTER (FEU-84-3) sections respectively. HAMAMATSU R-5600 had silica windows, whose transparency does not degrade under the typical HERA – B irradiation. Insensitivity to the magnetic field and high linearity of response in the requested range of anode currents were guaranteed by a mesh dynodes system. The other PMs were protected from magnetic fields by steel PM housings with special cylindrical screens made of permalloy. Relevant characteristics for all types of PMs together with the main environmental parameters are presented in the Table 2.

The PM power supply [7], or base, was designed on the basis of the Cockroft-Walton (C-W) multiplier [8] ideal for keeping the PM performance within design specifications at the high pulse rates needed for HERA – B (mean PM anode current can achieve 0.1 mA). It is

	R-5600U-06	FEU-68	FEU-84-3
Max rad. dose (kGy/y)	15	4	1
PhC operating range (nm)	160-650	300-850	300-820
PhC sensitive spot ϕ (mm)	8	10	25
PhC material	quartz	borosilicate glass	borosilicate glass
Number of dynodes	8	10	12
Max operating gain $\times 10^5$	1.4	0.4	2.4

Table 2
PM and Photocathode (PhC) parameters

moreover inexpensive, simple in exploitation and, finally, has low power dissipation, especially important for the tight geometry and absence of a cooling system in the INNER section. High radiation tolerance of the circuitry was achieved by using a limited number of active components and ensuring non-sensitivity of the circuit to the degradation of the components crucial parameters.

During the full HERA – B lifetime the PM/C-W system showed an excellent reliability. The rate of malfunctioning did not exceed 0.1% per month, adding up to less than 1.3% after more than one year of continuous ECAL operation without any intervention. Among all PMs installed the non-linearity mean values were -0.24% (RMS=0.59%) for FEU-68 and -0.22% (RMS=0.64%) for FEU-84-3. All R5600 preserved a linear response in full dynamic range of current amplitudes.

3.2 HV control

The ECAL Common High/Low Voltage (HV/LV) Control System distributed feeding voltages to the PM supplies, addressed them individually in order to control the PM amplification and to preserve the entire system of supplies from overcurrent. For the MIDDLE/OUTER sections a matrix-like individual PM addressing scheme was implemented. A different solution was used in the INNERMOST/INNER sections due to the tight geometry. The selection of individual PM channels inside a module was done by an intermediate board located at the rear of each module and carrying the phototube power supplies (see Fig. 5).

The voltage/control signals distribution electronics resided in 6 crates under ECAL each serving the left/right half (with respect to the proton beam pipe) of a particular calorimeter section. Each crate hosted one board to select the Y-coordinate (MIDDLE/OUTER only), and several identical boards to distribute

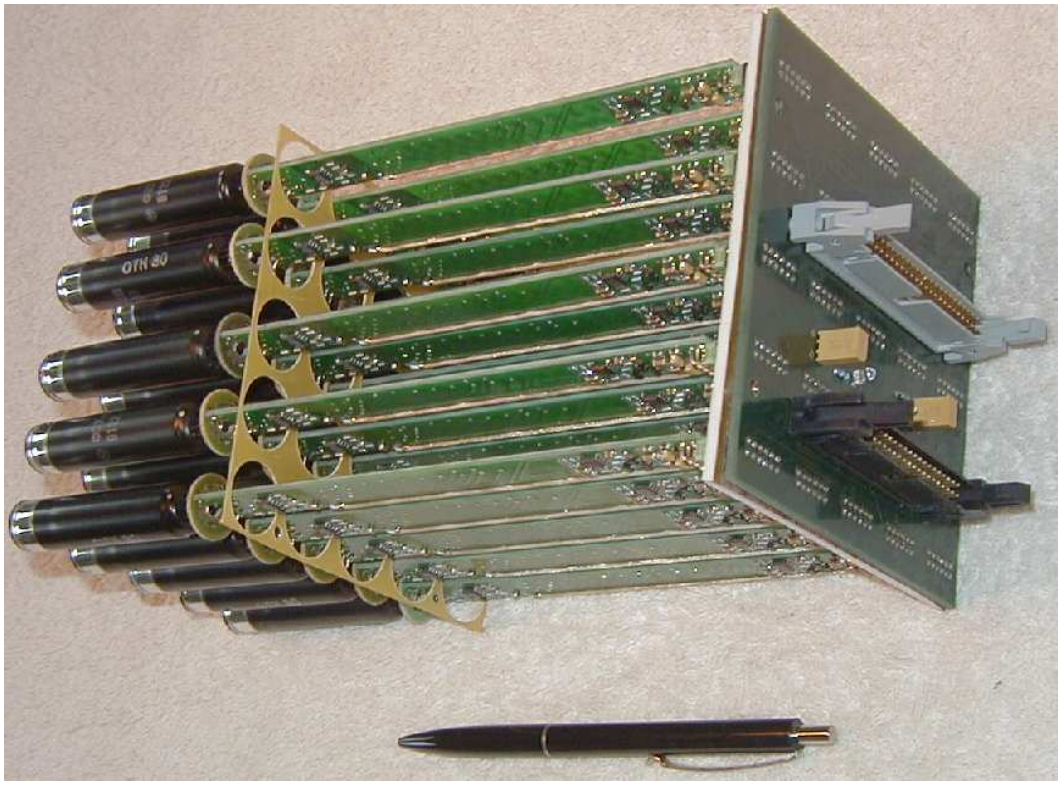

Fig. 5. Photograph of the distribution board equipped with FEU-68 phototube-supply doublets.

high/low voltages and control signals to groups of C-W bases. Individual output channels on each distribution board were protected from overcurrent in +100 V power source. The crate was administrated by a passive controller board, responsible for all VME communications with the control board, located in the unlimited access electronic hut and used to program X/Y-address of the PM HV supply, send DAC pattern and examine overcurrent-protection circuits. Each HV/LV control system had 3 types of DC power sources: +6 V, -6 V and +100 V. Low voltage sources (+6 V, -6 V) resided under the calorimeter in the low level radiation area and could be controlled remotely from the electronic hut. Moreover a distinct LV source -5 V, common for all passive controllers, feeded circuits responsible for receiving signal from the control board. These chains were decoupled from the rest of controller circuitry by means of optrons to avoid grounding loops. All +100 V sources were located in the electronic hut.

During several years of HERA – B continuous operation no malfunctions of the high/low voltage control system as well as any performance degrading was observed. The system proved to be very reliable, easy-to-operate and fully adequate to its purposes. The overall system power consumption from +100 V sources proved to be low: average currents $\sim$0.2 mA/C-W were observed with all PM high voltages set up and

no beam in the accelerator. Average value of LV consumption was ∼10 mA per channel.

3.3 ECAL monitoring system

The ECAL monitoring system was designed to:

(1) perform readout chain functionality control;
(2) monitor the long-term stability of individual readout channel (dominated by the PM gain stability) at the level of 2-3%;
(3) emulate physical signals in a required range of input amplitudes for ECAL pretrigger testing purposes.

Each readout channel was equipped with a distinct independently operated LED. This allowed to configure an arbitrary pattern of flashing LEDs (LED pattern) on the detector. The LEDs monitoring all channels of one ECAL module were controlled by a *LED driver board* which provided feeding voltages and allowed to configure the LED pattern. The LED pulse shape was similar to the physical signal being its duration compatible with the signal collecting time of 60 ns. The addressing of the channel inside a module was done via a dedicated shift register storing the LED pattern to be fired.

ECAL regions equipped with FEU68 and FEU-84-3 were instrumented with relatively cheap red LEDs L934SRCB with 660 *nm* emitting wavelength and 300 *mcd* brightness, compatible with the corresponding photocathode performance. Being the R-5600 photocathode not sensitive enough to red light to provide response in the full demanded dynamic range, more expensive bright blue Marl LEDs were employed, emitting at 450 *nm* and with a brightness of 600 *mcd*. In this case the output signal was a steep function of the voltage supplied. In order to maintain good stability and fine adjustment of LED signal, the corresponding driver board allowed an additional fine tuning of the light signal magnitude by means of controlled duration of the fire-signal (8 programmable steps in the range 5÷12 ns).

All LEDs were subdivided into 16 sectors each served by a devoted arm of the monitoring system and embracing 7x21 modules. The signal magnitude could be varied simultaneously for all channels in one sector in a range covering the full readout ADC dynamic range. The distribution of the control signals along LED drivers was organized according to a matrix-like addressing scheme similar to the one for HV/LV Control System. LED driver boards were nodes of a net system of cables used to deliver all necessary voltages to the corresponding modules. From the other side, cables were connected to the LED distribution boards (one per sector) delivering all necessary voltages and fire signals to the slave drivers, as well as the reproduction of the desirable LED pattern. Time spread in the delivery of fire pulses within one sector was less than 3 ns entirely depending on cable length.

Each distribution board was controlled by directives from a distinct control board, of the same design as the HV/LV Control System ones, located in the electronic hut and used to configure the LED pattern and the reference analog voltage needed to vary pulse magnitude. The LED power supply system included 8 distinct sources -6 V (type EWS-300-6), each of them feeding 2 sectors of the calorimeter (vertical band 2 x 1/16 part) and 16 independent regulable positive power sources (one per sector). All of them were placed beneath the calorimeter and were connected to the LED distributors via copper buses. Current consumption could achieve up to 8 A/sector from the adjustable power source and up to 20 A/sector from the -6 V source. The LED control system organization is illustrated in Fig. 6.

During the data taking the LEDs were fired with a frequency of about 10 Hz in coincidence with the empty gap of 15 consequent non-filled HERA bunches. This allowed tracing individual channel stability directly during the data taking without interfering with it. The long-term stability of the ECAL readout chain was measured by means of the monitoring system to be within 2%, in accordance with what evaluated by means of physical signals as π^0 and η mass ($< 3\%$) or E/p position ($\sim 3\%$) [9] and compatible with the design specifications.

Adjustment of the LED timing was performed thanks to a VME programmable *Test Pulse Board* and it was aimed to align it, together with the ECAL front-end and the ECAL pretrigger systems to the full HERA – B DAQ system using the delayed input trigger signal called *first bunch-crossing (1BX)*. Further delays could be obtained by means of coarse and fine adjustments, the first (0:255BX) being used to select successive bunch-crossings, and the second one (0:128 ns in step of 2 ns) allowing to perform fine LED signal synchronization with respect to the front-end drivers gates.

4 The readout electronics

The ECAL readout (RO) system [10] was designed to handle the analog signals of the 5956 PMs and consisted of 226 electronics cards. Its main logic functions were:

- to provide a fast signal digitization ($96\ ns$);
- to format and transmit the data for the ECAL pre-trigger (EPT) system;
- to format the calorimeter event and transmit it to the HERA – B Second Level Processors farm and to the reconstruction farm.

The global scheme of the designed RO boards is shown in Fig. 7. The RO card was built on a 9U VME standard and was formed by two parts:

- a mother board containing all the digital circuitry;
- a modular analog part consisting of independent units (ADC SECTION) to be plugged into the mother board.

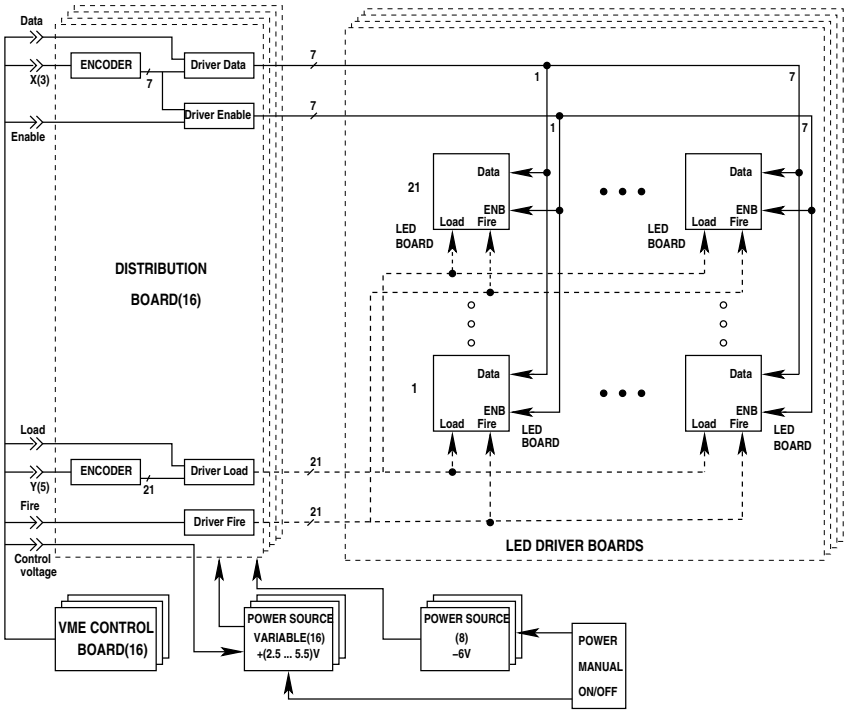

Fig. 6. LED control system block diagram.

Such modular design was an important feature of the system in order to keep separated, as far as possible, the analog and digital circuitry and to allow easy replacement of the faulty analog cards.

Each board could read out a maximum of 32 channels and was plugged into a crate with the backplane using the two free rows of the connector P2 (the central row being dedicated to VME signals) as a private bus for the HERA – B Fast Control System (FCS [11]). This bus, which was driven by an FCS daughter card, distributed the machine global timing signals, such as the Bunch Crossing (BX) Clock (96 ns period, 10.4 MHz frequency) and all the signals relevant to the First Level Trigger (FLT [12]) to the RO board.

In order to ensure the needed energy and spatial resolution in the energy range $0.3 \div 200\ GeV$ (energy released by the minimum ionizing particles, MIPs, used for calibration and maximum energy release by the electrons from J/ψ decay respectively), a 12 bit digital linear conversion of the analog signals was used in the whole calorimeter, except for the INNERMOST section, where such requirements could be met only by a 13 bit effective conversion obtained with a signal compression (non linear option). The noise level was at the level of one ADC channel ($0.5\mu V$) RMS in order to benefit of the full dynamic range of the conversion. The design of the ADC SECTION was such that both 12 and 13-bit options could be achieved by simply adding or removing a few components. The scheme reported in Fig. 8, which we will use for the following description, refers

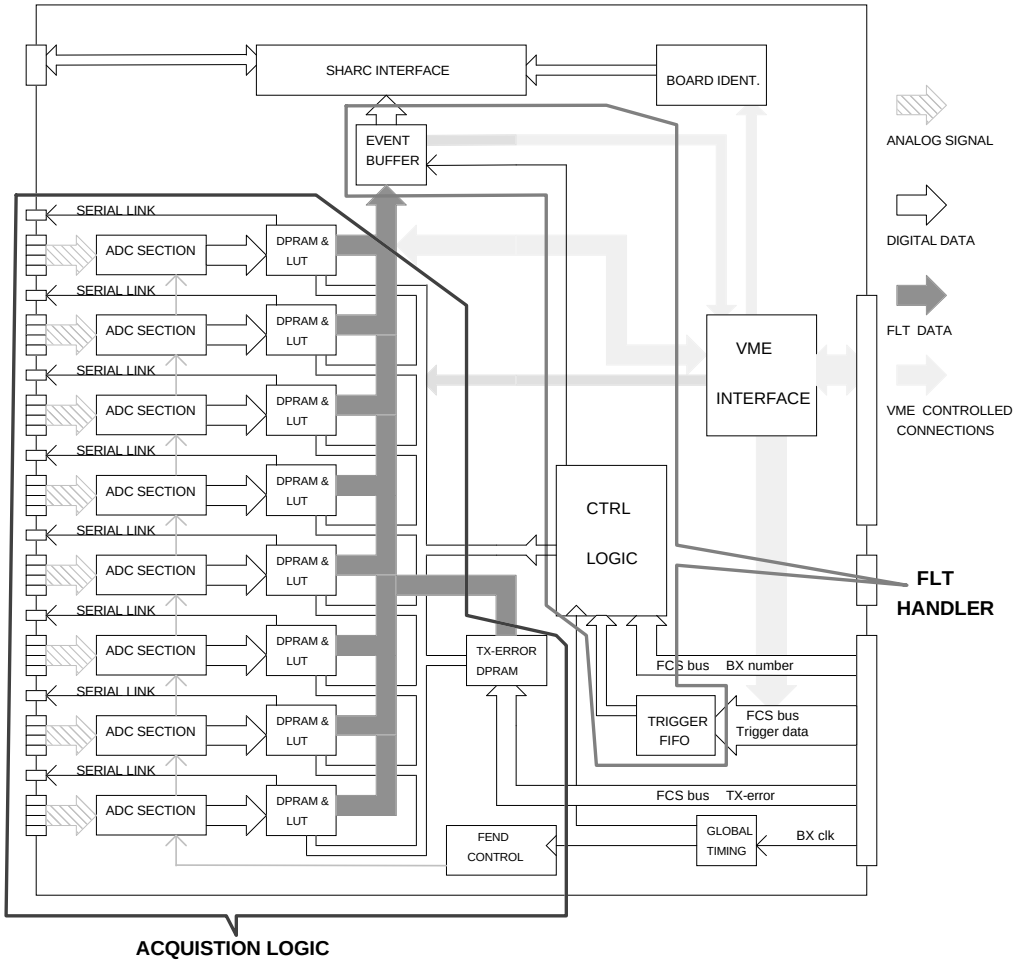

Fig. 7. Global logic scheme of the ECAL readout board.

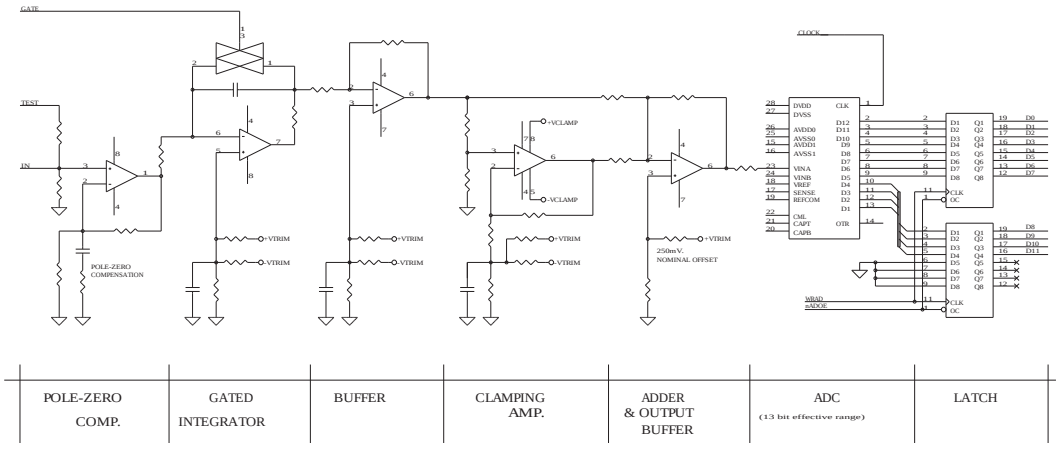

Fig. 8. ADC SECTION logic scheme.The block scheme refers to the 13 bit (non linear) transfer function version of the ADC.

to the non linear option.

Signals from the PMs were transmitted through $\sim 40\ m$ long coaxial cables to the ADC SECTION where they were buffered and pole-zero compensated, to recover the cable attenuation, and then fed into a gated integrator. The gated integrator, in coincidence with the BX clock, performed a 60 ns integration (to allow for a complete charge collection) of the signal and then a 36 ns discharge of the integrating capacitor. In order to get the signal compression the shaped signal was split into two branches and successively summed together (two slopes method). In the first branch the signal traveled unaffected, while in the second it was fed into a 100 MHz bandwidth clamping amplifier. With this compression technique it was possible to gain one bit in the transfer function. The signal was then sent into the ADC sampling at a rate of 10 $Msps$.
The 12 bit linear transfer function version of the ADC SECTION was simply obtained by eliminating the clamping amplifier branch.

Data coming from each ADC SECTION were stored at the BX rate into a Dual Port RAM (DPRAM) organized as a 256 events deep circular buffer in order to keep the information until a trigger decision was taken (FLT-accept). At the same time the ADC content were fed into a look-up table (LUT) to produce the compressed data required by the electron pretrigger (EPT) processors. The LUT output data were then serially transmitted (on a 2 wire/channel, 40MHz, differential TTL link) to the EPT board (SERIAL LINK).
The RO board was equipped with a single FIFO output buffer (EVENT BUFFER) where the FLT-accepted data from the DPRAM were transferred pending its transmission to the second level buffer (SLB) processors farm. The FLT accepted event identifiers coming from the FCS were stored into an additional TRIGGER FIFO, to increase the FLT peak rate handling capabilities of the board. The EVENT BUFFER and TRIGGER FIFO related logic allowed processing of up to seven consecutive FLT accepts (i.e. accepted events separated by a number of BXs smaller than the FLT pipeline depth). The FLT accepted data were then fetched from the EVENT BUFFER and transmitted to the downstream data acquisition (DAQ) processors (ADSP 21060 SHARC-based SLB) by means of the dedicated 80 MHz bus (SHARC LINK). The SHARC INTERFACE handled the shipping of the FLT accepted data over the SHARC LINK.
The GLOBAL TIMING section generated all the timing signals, phase locked to the BX clock, needed for DAQ, readout and diagnostic.
The front end control section (FEND) handled the analog to digital conversion and storing signals (integration gate, ADC clock, bus enable and DPRAM channels mapping).
The board was also capable of responding to other general purpose FCS commands (as global reset or test pulse issuing requests).

The RO board featured a VME interface allowing LUTs loading and extensive diagnostics. To this purpose

the board included facilities for selectively pulsing each channel with programmable level pulses and for injecting digital data at various steps of the acquisition process.

5 The pretrigger system

The ECAL pretrigger (EPT) system was used to seed the FLT with the electromagnetic cluster candidates relevant for the physics goals of the experiment, i.e.:

- electrons from J/ψ, Υ, b and c-quark semileptonic decays;
- photons with high transverse energy E_T ("hard photon trigger").

5.1 EPT algorithm

The designed system was based on the strategy adopted in the clusterization algorithm (see Sect. 6). Monte Carlo simulations showed that, due to the high tracks density of the experiment, a high efficiency on selecting electron clusters and a high rejection of the background could be achieved with an algorithm able to:

- perform a clusterization based on a 3×3 matrix of readout cells centered around the cell with the maximum deposit of energy;
- perform the recovery of the energy possibly radiated for bremsstrahlung by the electron/positron in the region before the magnet.This last point was shown to gain a relative 10% factor on the absolute EPT algorithm efficiency for J/ψ detection.

Some simplifications in the algorithm, like to operate with three independent calorimeter sections were shown to be acceptable (efficiency loss for electrons from J/ψ decay of $\sim 5\%$).

Starting with these considerations, an algorithm was developed, able to operate both at the readout and pretrigger levels. Its data flow can be summarized as follows:

- readout board level:
  - flag the calorimeter cells having an energy release above a preset threshold;
  - code the single cell absolute energy release and flag in a byte to be transferred to the EPT.
- pretrigger board level:
  - store the about 6000 bytes from the readout for each BX;
  - select the addresses of the cells having the flag set and corresponding to local maximum release of energy (central cell);
  - fetch the energy values of the eight calorimeter cells surrounding the central cell in a 3x3 matrix;
  - for the selected nonet calculate:
    a) the total cluster energy;
    b) the cluster center of gravity corrected for the electromagnetic cluster shape (S-shape correction).
  - select clusters having E_T greater than a preset threshold;
  - calculate the coordinates of the possible bremsstrahlung photon clusters and retrieve their energy

values (the electron/positron ambiguity can not be resolved by the pretrigger alone). The bremsstrahlung recovery feature is an original idea implemented for the first time at pretrigger level.

At the end of the algorithm a message was formed, containing all the relevant quantities to seed the FLT. Among them the energy information was crucial to correctly address the FLT track finding procedure. Therefore an absolute calibration had to be available already at this level. In Fig. 9 the invariant mass distribution of two pretrigger candidates in one board is shown as measured by the EPT energy and position information, where a clear $\pi^0 \rightarrow \gamma\gamma$ peak is evident at the correct position.

The designed system was completely pipelined and capable to process up to three candidates per BX per pretrigger board with a total latency of $\sim 3.5\mu s$ (35 BX) sufficient in order not to loose events up to a target interaction rate of $\sim 40\ MHz$.

5.2 EPT structure and protocol

The overall system consisted of 128 boards, processing the 5956 readout channels, developed on VME 9U boards. The global scheme of the EPT boards is shown in Fig. 10 while a complete description of the EPT and of its performance can be found in [13].

All EPT operations were driven by

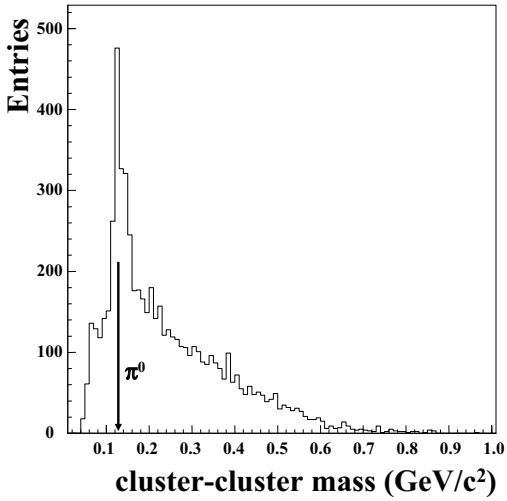

Fig. 9. Two cluster invariant mass measured using the energy and position information of the EPT only.

a 42 MHz (4 cycles each BX) "Fast Clock" locally distributed all over each card and synchronized with the HERA clock.

The 8-bit input data (7 bits for coded energy release in each RO channel plus one flag bit for energy deposit over a preset threshold) were transmitted by the readout cards, according to a serial synchronous protocol, on two lines per channel. Each card could manage signals from one RO board plus the border cells, distributed via passive patch panels, in order to completely map the whole calorimeter.

The Local Maxima Finder Unit (LMFU) analyzed the incoming serial data and flagged the channels with an energy deposit greater than all neighbors and over a preset threshold. The flagged channels were ordered by a Pipelined Priority Encoder (PPE), implemented into the LMFU logic block, able to process up to three clusters per machine

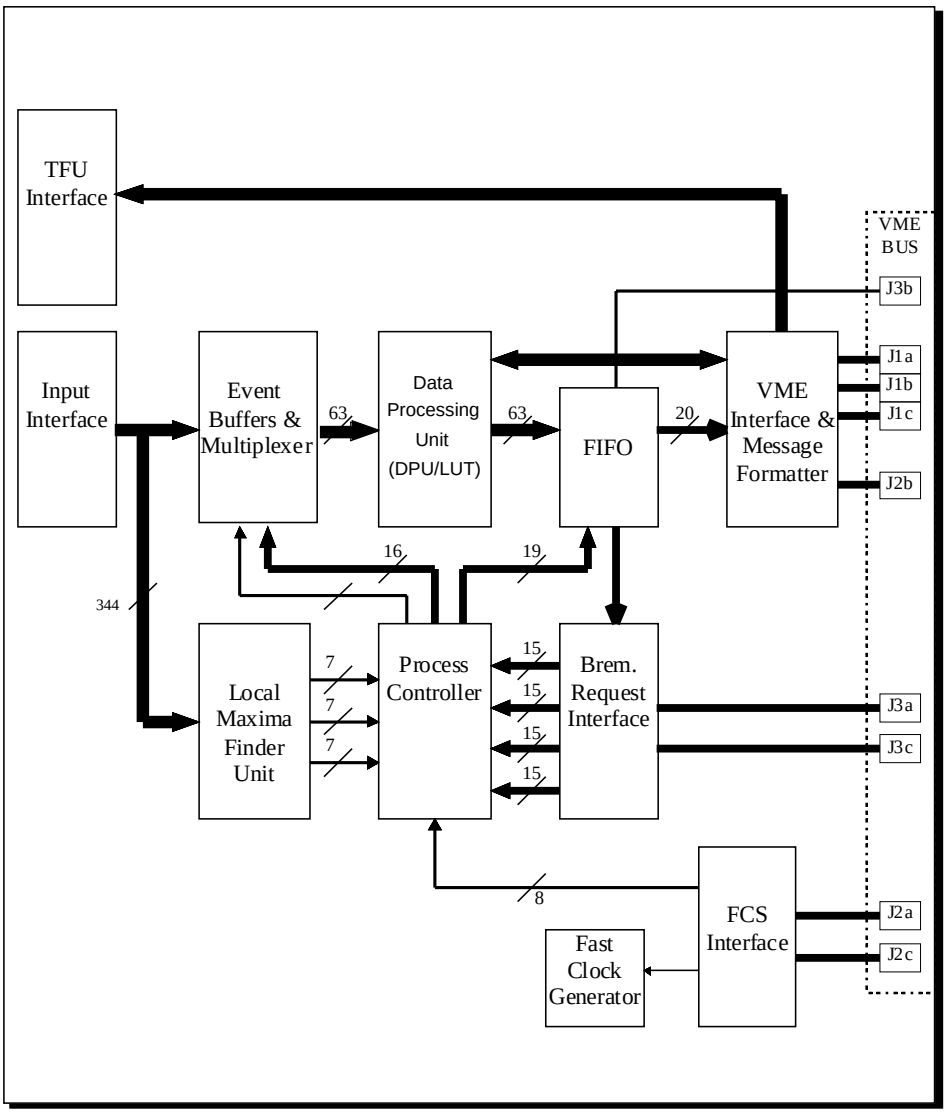

Fig. 10. Global logic scheme of the ECAL EPT board.

cycle. The cell number (6 bit) and the BX (8 bits) were used to address the Input Interface (IIF) Module for the cluster energy extraction, being the cluster a 3×3 cell matrix centered around the defined central cell. Data were sent by a Process Controller to the Event Buffer and Multiplexer (MUX) together with the coordinates of the cells of an eventual bremsstrahlung energy deposit. The MUX logic block provided these data to nine 7 bits buses for the Data Processing Unit (DPU). The whole processing in this block was performed via lookup tables (LUT). The relevant information provided by the LUT block were:

- cluster center of gravity (x and y);
- total cluster energy;
- coordinates of the possible bremsstrahlung photons;
- a flag if the total cluster energy exceeded a preset threshold;
- a flag if the total cluster transverse

energy exceeded a preset threshold;
- coordinates of the cells of an eventual bremsstrahlung energy deposit (a dedicated logic, the Bremsstrahlung Request Interface (BRI) guided the search for those cells and stored the relative information for further elaboration).

Finally, the FIFO outputs was connected to the pipelined Message Formatter (MF) formatting and storing the 80-bit data to be transferred to the first level Trigger Finding Units (TFU) via the TFU Interface logic block. Such transmission took place at a rate of 4 x 20 bit / BX.

The functioning of the system was continuously monitored during data taking by a server-client protocol based program providing online information about all relevant quantities elaborated by the EPT as energy depositions, candidate positions, trigger rates, latencies etc. Such quantities were continuously sampled and shown in histograms for the three ECAL sections. In case deviations from normal behaviour were observed, the information could be traced down to the single channel level. The system could quickly identify noisy channels dominating the trigger rate and mask them online in order to recover normal triggering conditions. In Fig. 11 the EPT rate is shown normalized to the interaction rate as a function of time, where a spike due to a noisy channel can be observed. The recovery of the normal trigger rate within a few seconds is due to the described online masking procedure.

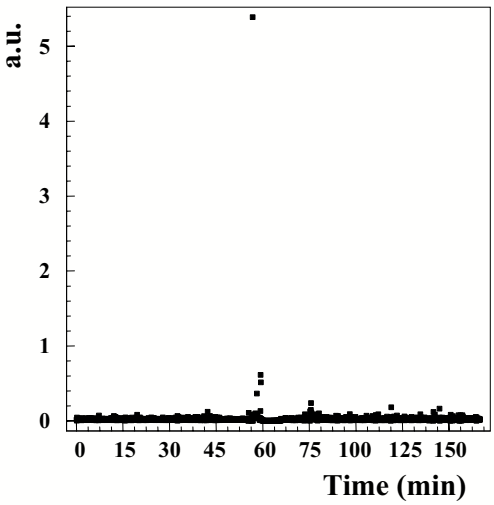

Fig. 11. EPT rate normalized to the HERA interaction rate (in arbitrary units) as a function of time.

5.3 Pretrigger simulation

In order to study the performance and efficiency of the ECAL pretrigger system, a dedicated package was developed [14] simulating the pretrigger on a bit level by using both Monte Carlo information and real data as input. Studies showed that the simulation was able to reproduce the pretrigger behaviour in deep detail.

In addition the simulation allowed to perform dedicated hardware tests of the pretrigger system by creating input data to be loaded into the pretrigger system out of Monte Carlo information. Operating the pretrigger and comparing the pretrigger output to the simulation results gave a fast feedback on the correct performance of the pretrigger system.

The overall efficiency of the pretrigger for the detection of the decay $J/\psi \rightarrow e^+e^-$ depended on several factors. Besides the geometri-

cal calorimeter acceptance and the overall reconstruction efficiency, the determining factors were the transverse energy threshold of the entire cluster and of its central cell. These were limited by the maximum input rate of trigger candidates that could be managed by the FLT as well as the reduction factors required by the further trigger levels. Moreover, as the pretrigger information was used to seed the FLT track search, also the spatial and energy resolutions determined the overall HERA – B trigger efficiency.
For the design of the FLT, it was assumed that, at an interaction rate of 40 MHz, the ECAL pretrigger could provide an average of two cluster candidates per bunch crossing at a rate of 8.52 MHz. This could be achieved via a cut on the transverse energy of $E_T \geq 0.7 GeV$. An overall efficiency for detecting the two electrons from J/ψ decay of $\sim 25\%$ was determined.

6 ECAL reconstruction

The ECAL reconstruction code [15] was used both in the off-line and online event reconstruction as part of the HERA – B high level trigger. Its main goal was to isolate and identify the clusters due to particles releasing at least $0.05\,GeV$ transverse energy in the calorimeter, in particular $e^{\pm}$ and γ and, moreover, to provide a reliable particle identification for electron-hadron discrimination.

Very different constraint were imposed to the reconstruction when used for trigger decisions (in particular very stringent time limits and high efficiency) or off-line, where a more time-consuming algorithm could be afforded in view of a more precise signal reconstruction. For this reasons a C++ object oriented code was developed in such a way to be included in the general reconstruction of the experiment and, in a simplified version, in the general trigger software.

The following main considerations guided the ECAL reconstruction code design:

- constraints: the code had to run with different time and accuracy performance at the trigger level, where a decision on the event had to be taken within $\sim 20\ ms$, and at the reconstruction level, where basically no time limits were imposed. Moreover the algorithm had to be very efficient on the interesting physics channels, with very small cross sections compared to the total inelastic one;
- working conditions: the calorimeter was hit by about 100 particle per interaction, releasing a signal in more than 10% of the ECAL cells. This implied that the probability for overlapping signals from different particles was not negligible, in particular in the INNER part of the detector, and the code had to be able to provide the best separation and reconstruction possible in such difficult conditions;
- interplay with the general HERA – B reconstruction: the ECAL reconstruction could profit from the information coming from other

detectors (in particular the tracking system), and vice versa. This imposed a modular structure able to communicate at each step with the other reconstruction/trigger codes.

Following these prescriptions, the code was designed in three main logical steps:

- pattern recognition: this included hit selection, clustering and shower reconstruction based on the ECAL information standalone;
- matching with tracks: the tracking system information was used in order to identify charged particles;
- final reconstruction: the final cluster-track association was performed and an identification provided (electrons, γ, hadrons, MIPs). Moreover the main parameters of the clusters/tracks were provided, as the position on ECAL (S-shape corrected center of gravity of the cluster [16]), the energy release, the presence of an associated bremsstrahlung cluster, the e/π discrimination.

The clustering phase was based on a variant of the hierarchical clustering method [17] which has the property that the time needed to scan and group in clusters all the N hit cells in the event is proportional to $N\ \log N$, thus limiting the computing time in case of high occupancy. Great care was payed to the clustering also for what concerns the algorithm separation power of neighbouring clusters sharing part of the cells. The energy of the shared cells is split among the close-by clusters in fractions proportional to the cluster energies. This usually small correction to the cluster energy has a marginal impact on the energy resolution, but helps significantly to improve the spatial resolution of partially merged clusters, since the corrected center-of-gravity algorithm is sensitive to the details of the small lateral deposits. Fractioning of common cells proved therefore to be crucial for increasing the γ-γ separation power at high π^0 energies (see Sect. 8).

Another important task of the reconstruction algorithm was to allow for a precise calorimeter calibration. The full procedure applied in order to obtain the desired calibration level is described in Sect. 7. The performance of the reconstruction in terms of energy and position resolutions, which depend also on the detector design and behaviour during the data taking, are discussed in Sect. 8.

7 ECAL calibration

A calibration precision at the level of few percent had to be reached in the whole calorimeter in order not to spoil the experimental resolution on the physical states of interest, fully dominated by the material in front of the calorimeter. Moreover an energy calibrated information had to be available already at pretrigger level, with a precision sufficient to provide the correct regions of interest to the Kalman Filtering FLT processors for the electron candidates search.

In order to be able to perform cal-

ibration adjustments frequently in time and in short dedicated data taking, most of the calibration procedure was foreseen almost independent of other detectors, leaving to the offline analysis the duty to refine the results by adding the tracking system information. Given the large number of ECAL cells to be calibrated and the required precision, a multi-level calibration scheme was adopted, including:

- PM gain pre-calibration in the laboratory;
- equalization of ECAL occupancies in each cell;
- absolute calibration on physical signals ($\pi^0 \to \gamma\gamma$);
- calibration check and refinement using MIPs and other signals as the η particle;
- ECAL-tracking combined calibration using E/p peak position.

The pre-equalization consisted in a PM gain adjustment in order to have similar response to a given LED light amplitude from all cells. This procedure did not provide an absolute calibration.

The occupancy equalization step allowed to reach a relative intercalibration of nearby channels at the level of 15% by studying the fraction of events with energy above a given threshold as a function of the distance from the beam pipe, and adjusting the calibration constant of each cell in order this fraction to be in agreement with Monte Carlo predictions. The precision obtained and the level of determination of the absolute energy scale was still not sufficient, after this first step, for the described requirements.

The following step of calibration was performed on physical signals to provide an absolute cell by cell calibration. It was chosen to perform such step using the π^0 particles as:

- they are copiously produced in pN interactions ($\sim 8\pi^0/BX$) and no special trigger requirements are needed in order to produce a high statistics ($\sim 10^7$) in a short (~ 1 hour) time over the whole ECAL;
- their reconstruction does not need any information from other detectors (fast stand-alone acquisition in dedicated runs sufficient) ;
- their energy spectrum spans over a large range (up to $\sim 100\ GeV$), being the upper value limited by the ECAL γ-γ separation power.

The concept of the method consisted in building, for each (i-th) ECAL cell, center of the γ_i cluster, the $\gamma_i\gamma$ mass distribution obtained by combining γ_i with all other γ in the event. In this way for each cell i the mass position of the $\pi^0 \to \gamma_i\gamma$ could be extracted by fitting the distribution with a function for the signal (gaussian-like) and a polinomial one for the combinatorial background and the calibration constant of this cell adjusted in order to obtain the nominal π^0 mass. The procedure was then repeated iteratively until the best approximation to the nominal mass could be reached in all cells. During iterations not only the mass position but also the width of the π^0 signal improved. In Fig. 12 the starting and final mass distributions are shown for all ECAL cells to-

gether, showing an improvement in the π^0 width from $\sim$ 17 MeV/c^2 to $\sim$ 10 MeV/c^2. Moreover the η signal becomes visible after calibration only.

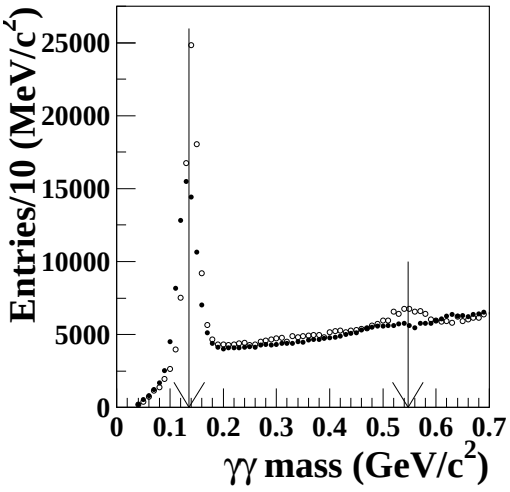

Fig. 12. γ-γ mass distribution in the π^0 and η region before (black circles) and after (open circles) the π^0 calibration procedure. π^0 and η signals are marked with arrows.

The calibration procedure was then completed by two more steps aimed to improve the precision in the high occupancy regions where it was difficult to observe a clear π^0 signal due the large background levels.
The first step was based on the detection of MIPs (mainly muons) which release in the calorimeter an energy equivalent to a $\sim$ 0.3 GeV electromagnetic shower. In Fig. 13a) the energy spectrum released in ECAL by muons from J/ψ decay triggered by the muon detector is shown, while in Fig. 13b) the stability of the MIP peak position is shown, run per run, in a time scale of about 6 months. A stability in time of the overall calibration at the level of 2.5% can be observed (see Fig. 13c)).

The second step was also performed at the off-line level. The electron momentum information from the tracking system was used in order to monitor the peak position of the energy to momentum (E/p) ratio. For electrons/positrons this distribution is expected to be peaked near one. In Fig. 14 a typical E/p is shown separately for the INNER (a), MIDDLE (b) and OUTER (c) sections, using electrons from J/ψ decay. As expected a mean value $< E/p > \sim 1$ was found while typical values for the width of the distributions are $\sigma_{E/p} \sim 6\%$ for the INNER and MIDDLE sections and $\sigma_{E/p} \sim 7\%$ for the OUTER, mainly due to the material distribution in front of the calorimeter and the intrinsic performance of the detector.

The use of all the described methods allowed to obtain a final calibration precision $< 2\%$ in the whole calorimeter. Such information was used in the Monte Carlo in order to provide a realistic simulation of the ECAL calibration.

8 ECAL performance

The performance of the electromagnetic calorimeter were studied using the large data sample acquired during the physics data taking in the year 2002-2003. Large samples of π^0, η and J/ψ were selected by means of the ECAL information. This allowed to determine the main parameters of the calorimeter, namely:

- the spatial resolution;

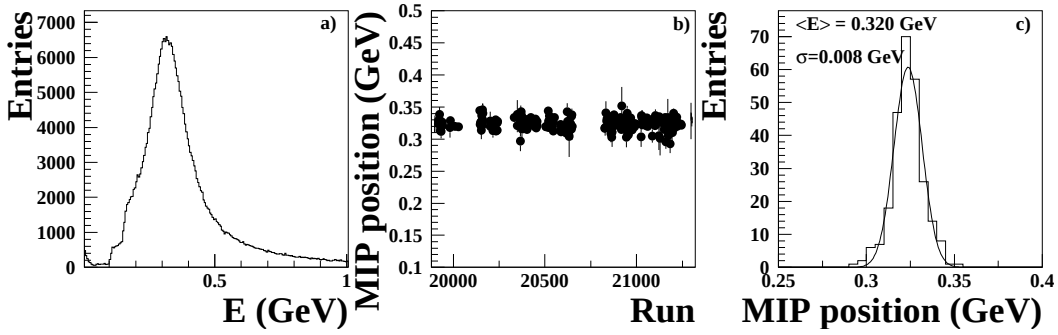

Fig. 13. a) signal released by triggered muons in the calorimeter. b) MIP position as a function of run number. c) distribution of MIP position for all runs fitted with a gaussian.

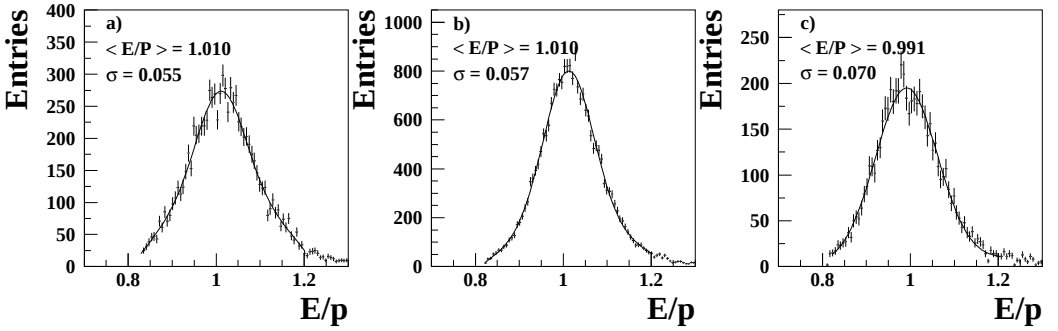

Fig. 14. E/p distributions for the INNER, MIDDLE and OUTER section of the calorimeter. Electrons and positrons from J/ψ decay are used.

- the energy resolution;
- the light yield non-uniformity;
- the $\pi^0 \rightarrow \gamma\gamma$ separation power;
- the readout stability.

The spatial resolution was determined by selecting a highly purified electron/positron sample from J/ψ decay obtained with the following requests: $E/p \sim 1$ and tag given by the emission of a bremsstrahlung γ. The measured center of gravity of the cluster was compared to the information provided by the tracker as a function of the energy. The ECAL energy resolution was determined, using γ from π^0 and η decay, by studying its contribution to the width of the signals as a function of the measured γ energy. In Fig. 15 the dependence of $\frac{\sigma_E}{E}$ and of the spatial resolution σ_{xy} are shown separately for the INNER, MIDDLE and OUTER sections. In Table 3 the values for stochastic and constant term are reported for both quantities. The measured resolutions were compatible with what expected at technical design and project.

The light yield (l.y.) non-uniformity was determined studying the $\pi^0(\rightarrow \gamma\gamma)$ peak position as a function of the distance $\Delta r = r_{cog} - r_{cent}$ of the γ cluster center-of-gravity to the center of the cell. From the observed π^0 mass value the relative distortion of the measured cluster energy as a function of Δr could be obtained. A maximum non-uniformity of re-

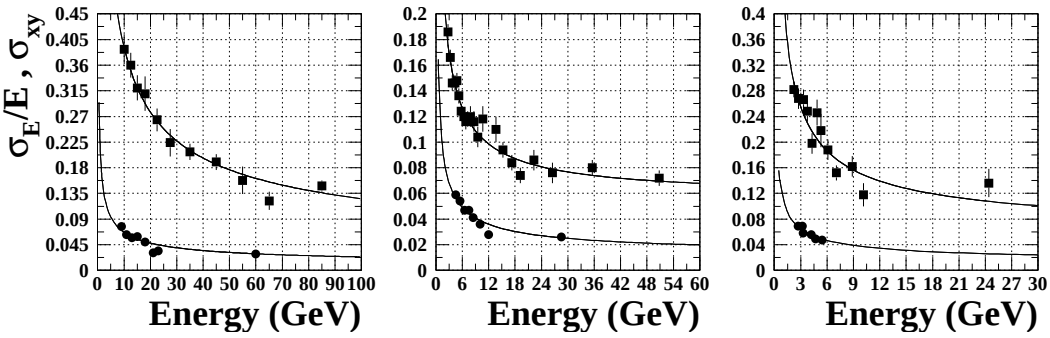

Fig. 15. Energy resolution $\frac{\sigma_E}{E}$ (circles) and spatial resolution σ_{xy} in cm (squares) as a function of the measured cluster energy in the INNER (left), MIDDLE (center) and OUTER (right) sections. For MIDDLE and OUTER σ_{xy} points are rescaled by a factor 5 for visualization.

sponse of $\sim$ 10% was observed for all modules close to their edges as shown in Fig. 16. Such effect could be corrected with an iterative procedure similar to the one used for π^0 calibration and position-dependent correction functions were determined to be used in the off-line reconstruction in order to optimize the energy and position measurements. An improvement on the π^0 and η resolutions as much as 20% were achieved with such corrections. In Fig. 17 the η signal is shown before and after the non-uniformity correction: such signal is also used to verify the calibration procedure as γ from η decay span a larger energy interval with respect to the ones from π^0.

As pointed out in the reconstruction section, a crucial feature of the used clustering algorithm was the fractioning of the hit cells common to two neighbouring clusters (merged clusters). This had a dramatic impact on the γ-γ separation power and thus on the capability of reconstructing π^0 of higher energies. In Fig. 18 the efficiency on π^0 reconstruction is shown as a function of the γ-γ opening angle. As it can be seen, full efficiency was still obtained at angles smaller by a factor of two (i.e. double π^0 energy) as compared to a standard non optimized algorithm. In the same figure the π^0 signal reconstructed using merged clusters is shown compared to the total π^0 signal, showing no evident mass distortion.

9 The bremsstrahlung PID method

An original PID method, implemented both at pretrigger and reconstruction levels, was based on the identification and recovery of the energy emitted by $e^{\pm}$ as bremsstrahlung (BR) γ when crossing the materials before the magnet (the energy depositions of γ emitted after the magnet were not separated from the $e^{\pm}$ cluster) [18]. In order to identify the BR γ, a cluster was looked for in the ECAL having the same coordinate (within the detector spatial resolution) as the $e^{\pm}$ candidate cluster in the non-bending plane and, in the bending plane, a

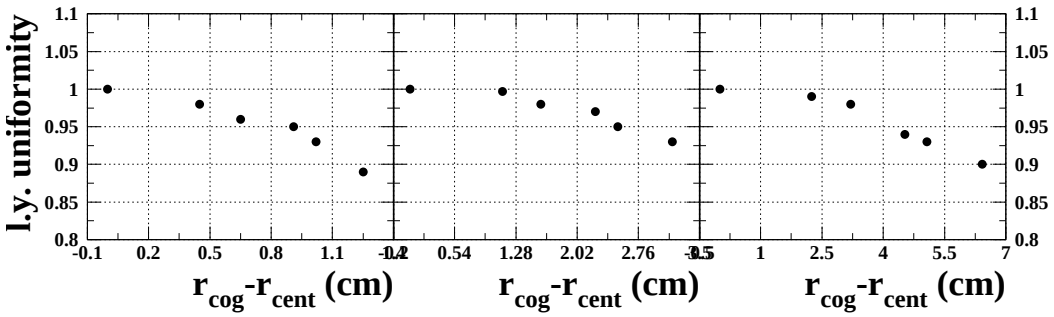

Fig. 16. Uniformity of response of the energy measurement in the INNER (left), MIDDLE (middle) and OUTER (right) ECAL modules.

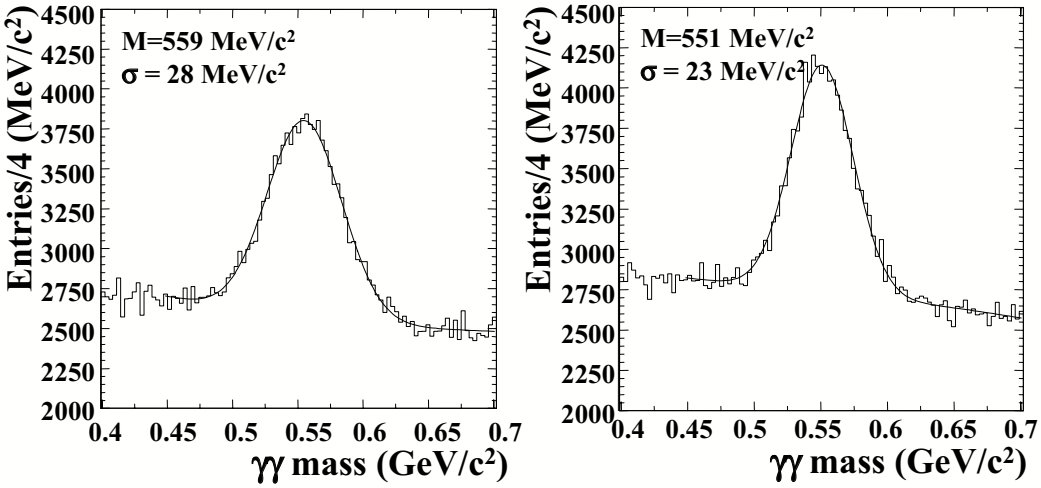

Fig. 17. η signal before and after the l.y. non-uniformity correction.

	INNER	MIDDLE	OUTER
$\frac{\sigma_E}{E}$ (%)	$20.6(.3)/\sqrt{E} \oplus 1.2(.2)$	$11.8(.2)/\sqrt{E} \oplus 1.4(.1)$	$10.8(.1)/\sqrt{E} \oplus 1.4(.2)$
σ_{xy} (cm)	$1.25(.03)/\sqrt{E} \oplus 0.022(.003)$	$1.37(.03)/\sqrt{E} \oplus 0.28(.02)$	$2.17(.09)/\sqrt{E} \oplus 0.28(.15)$

Table 3
HERA – B Main ECAL performance parameters. Energy expressed in GeV.

distance from it $\propto 1/E_{e^\pm}$, being $E_{e^\pm}$ the $e^\pm$ energy measured by ECAL (see Fig. 19). The main difference between the pretrigger and the offline reconstruction was that, while in the former it was not possible to resolve the left/right (i.e. electron/positron) ambiguity, in the latter this was removed by the charge information from the tracking system.

As hadrons do not emit bremsstrahlung, the method allowed a powerful electron tag and a hadron rejection additional to the standard E/p information. Moreover the recovery of the BR energy lost allowed a proper evaluation of the electron momentum at the interaction vertex position, improving the resolution on the physical signals. The effectiveness of the tagging algorithm is shown in Fig. 20

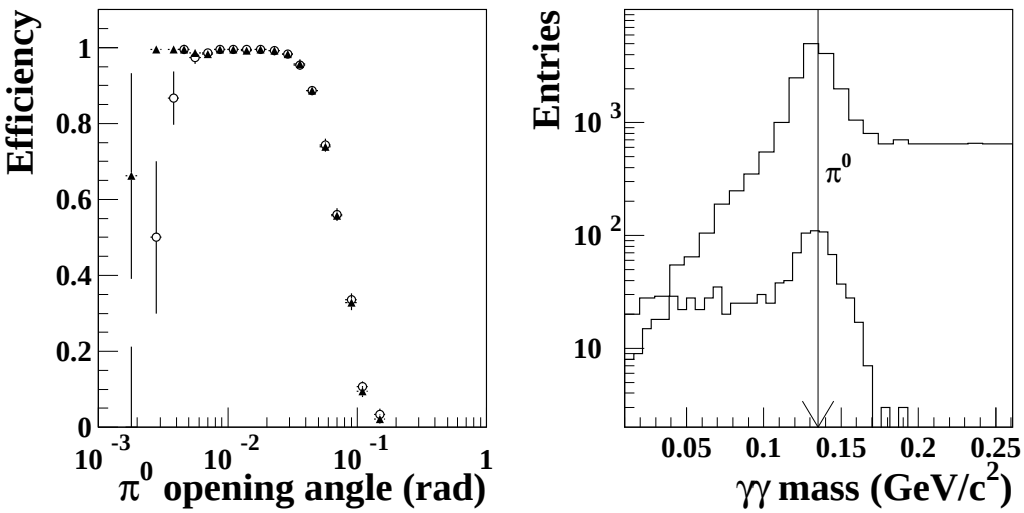

Fig. 18. Left: π^0 reconstruction efficiency as a function of the γ-γ opening angle for the used clustering method (triangles) and for clustering method not separating merged clusters (circles). Right: π^0 reconstructed from merged clusters (below) compared to the total π^0 signal (above).

where the J/ψ signal is shown without any BR tag (b) and requiring that one (c) or both (d) triggered electrons emitted a BR γ. The statistics scaled as $1 : 0.7 : 0.15$ with a signal over background ratio increase as $1.2 : 2.0 : 6.5$.

The method was used in all analyses requiring very clean electron samples.

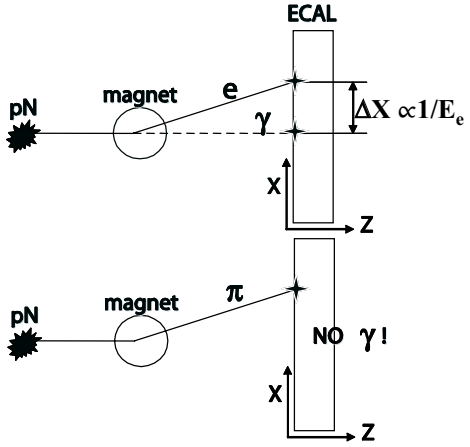

Fig. 19. Concept of the BR recovery method

10 ECAL physics achievements

ECAL played a crucial role in the HERA – B physics program. Apart from providing the di-electron trigger to the whole experiment, its information was used for all the studies concerning electron and gamma identification and reconstruction. These included:

- charmonium studies as J/ψ, $\psi(2S)$ and χ_c production and decay, polarization and differential distributions;
- measurement of nuclear effects in charmonium production (A-dependence);
- open and hidden b-quark production cross section measurements (Υ, $b \to J/\psi X$);

- direct γ, π^0 and η production in pN interactions.

Concerning the charmonium production studies, a total sample of about 130000 J/ψ, 2500 $\psi(2S)$ and about 6000 χ_c were selected by triggering on the decay electrons/positrons and after the full reconstruction and analysis selection. An overview of the main results concerning the charmonium studies can be found in [19]. In Fig. 20a) the full e^+e^- mass spectrum is shown where, other than the charmonium states, also the $\rho/\omega/\phi$ particles are evident in the low mass range. The J/ψ particle was observed with an experimental resolution of $\sim 60\ MeV/c^2$ (Fig. 20b)).

The χ_c sample (see Fig. 21), the largest world statistics in fixed target, was selected through the $\chi_c \to J/\psi\gamma \to e^+e^-\gamma$ decay channel requiring the additional detection of the γ from χ_c decay. This last information was also used for the observation of the independent $\chi_c \to J/\psi\gamma \to \mu^+\mu^-\gamma$ channel.

In Fig. 22 the e^+e^- mass spectrum of $b \to J/\psi X \to e^+e^-X$ decay is shown, while in Fig. 23 the same distribution is shown in the high mass interval, where the $\Upsilon \to e^+e^-$ signal can be observed. A detailed description of the results concerning these two channels can be found in [20] and [21] respectively. The HERA – B b production cross section measurement through the $b \to J/\psi X$ decay is the world most precise in fixed target.

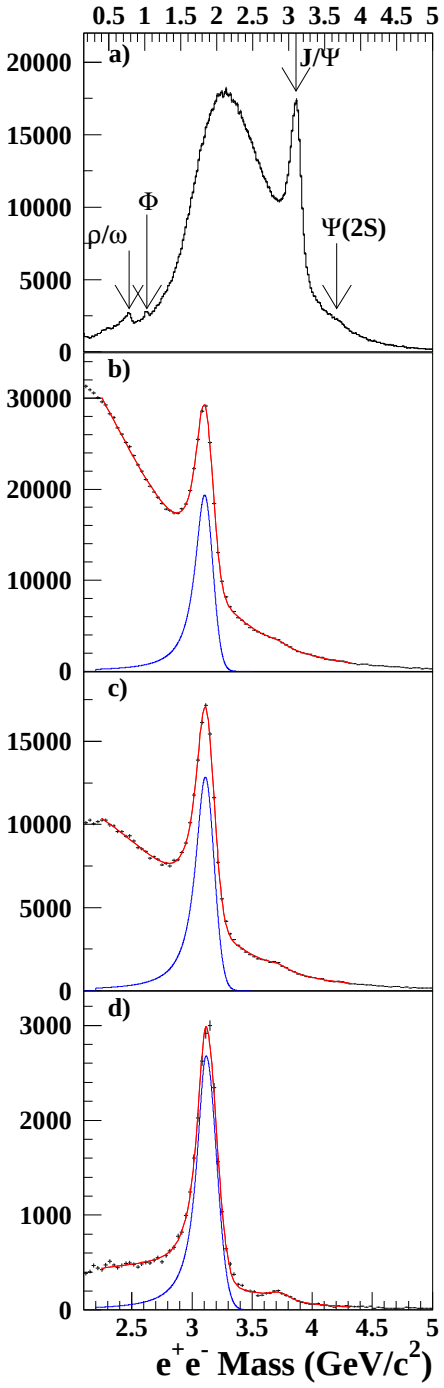

Fig. 20. e^+e^- mass spectrum. a) with low mass region. b)-d) J/ψ region without electron bremsstrahlung tag (b), with one or two (c) and two (d) tags. X-axis binning is 33 MeV/c^2.

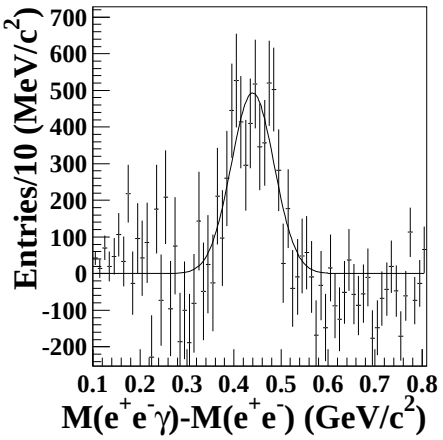

Fig. 21. The χ_c signal.

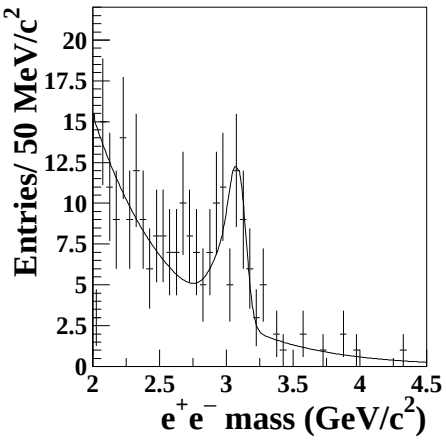

Fig. 22. The $b \to J/\psi X$ signal.

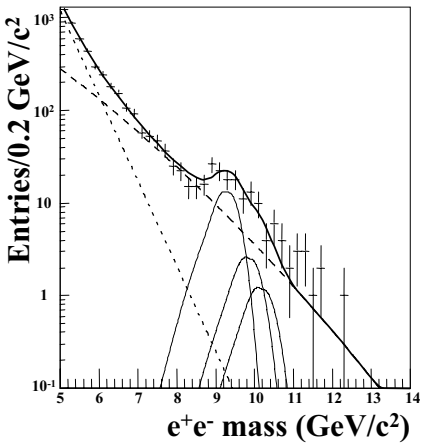

Fig. 23. The Υ, Υ' and Υ'' signals.

11 Conclusions

The HERA – B experiment performed a wide physics program mainly in the heavy flavor and charmonium production in pN interactions at high energy. A crucial part of the measurements performed involved the information of the electromagnetic calorimeter. The use of such device was crucial both at trigger level and in the reconstruction of reactions involving electron and gamma identification. During the whole physics data taking the behaviour of the electromagnetic calorimeter was stable with performance compatible with what foreseen at technical design and project.

HERA – B completed its physics program in the year 2003.

References

[1] HERA – B Design Report - DESY-PRC 95/01, January 1995.

[2] A. Zoccoli for the HERA – B Collaboration, Nucl. Instr. Methods **A446** (2000) 246

[3] M. Bruschi for the HERA – B Collaboration, Nucl. Instr. Methods **A461** (2001) 332

[4] The HERA – B Collaboration, Luminosity determination at HERA – B , submitted to Nucl. Instr. Methods A, arXiv:0706.0131v1.

[5] G. S. Atoyan et al., Nucl. Instr. Methods **A320** (1992) 144.

[6] E. Tarkovsky, Proceedings of the VI International Conference on Instrumentation for Experiments at ee Colliders, Novosibirsk, Russia,

1996. Nucl. Instr. Methods **A379** (1996) 515.

[7] G. Avoni et al., Nucl. Instr. Methods **A560** (2006) 539.

[8] H. Greinacher, Erzeugung einer Gleichspannung vom vielfachen Betrage einer Wechselspannung ohne Transformator, Bulletin des Schweiz. Elektrotechn. Vereins 11 (1920) 59.
H. Greinacher, Z. Phys. **C4** (1921) 195
J. D. Cockcroft and E. T. S. Walton, Proc. Roy. Soc. **A136** (1932) 619.

[9] G. Avoni et al., Proceedings of the IX International Conference on Calorimetry in High Energy Physics (CALOR 2000), Annecy, France, 9-14 Oct 2000. Editors B. Aubert, J. Colas, P. Nedelec, L. Poggioli, Frascati Physics Series 21 (2000) 239.

[10] B. Giacobbe et al., Proceedings of the VII International Conference on Calorimetry in High Energy Physics (CALOR 97), Tucson, AZ, 9-14 Nov 1997. Editors E. Cheu, T. Embry, J. Rutherfoord & R. Wigmans, World Scientifics (1998) 429.

[11] T. Fuljahn, Aufbau und Charakterisierung des schnellen Kontrolsystems fuer das Experiment HERA – B , Ph.D. Disseration, Univ. Hamburg, 1999.

[12] V. Balagura et al., Nucl. Instr. Methods **A494** (2002) 526.

[13] V. Alberico et al., Il Nuovo Cimento **110A** (1997) 1453.
C. Baldanza et al., Proceedings of the 7th Pisa Meeting on Advanced Detector Frontier Detectors for Frontier Physics, La Biodola, Isola d'Elba, May 25-31, 1997. Nucl. Instr. Methods **A409** (1998) 643.
B. Giacobbe et al., Proceedings of the VIII International Conference on Calorimetry in High Energy Physics (CALOR 99); Lisbon, Portugal, 13-19 June 1999. Editors G. Barreira, A. Gomes, A. Maio, B. Tom, M.J. Varanda, World Scientific (2000) 598.

[14] J. Flammer, Development of the ECAL pretrigger system simulation for the experiment HERA – B and analysis of efficiencies of the decay $J/\psi \rightarrow e^+e^-$, DESY-THESIS-2001-048, http://www.slac.stanford.edu/spires/find/hep/www?r=desy-thesis-2001-048.

[15] M. Villa et al., Proceedings of VII International Conference on Calorimetry in High Energy Physics (CALOR 97), Tucson, AZ, 9-14 Nov 1997. Editors E. Cheu, T. Embry, J. Rutherfoord & R. Wigmans, World Scientifics (1998) 537.

[16] L. Bugge, Nucl. Instr. Methods **AA242** (1986) 228.

[17] R. A. Devijver and J. Kittler, Pattern Recognition, A Statistical Approach, Prentice-Hall Int, Inc. London, 1982.

[18] B. Giacobbe et al., Proceedings of the IX Topical Seminar on Innovative Particle and Radiation Detectors (Siena 2004), Siena, Italy, 23-26 May 2004. Nucl. Phys. B Proc. Suppl. **150** (2006) 257.

[19] P. Faccioli et al., Proceedings of the II International Conference on

Hard and Electromagnetic Probes of High-Energy Nuclear Collisions (Hard Probes 2006), Asilomar, California, 9-16 Jun 2006, Nucl. Phys. **A783** (2007) E1.

[20] I. Abt et al., Phys. Rev. **D73** (2006) 052005.

[21] I. Abt et al., Phys. Lett. **B638** (2006) 13.